Catena 152 (2017) 242–251

Contents lists available at ScienceDirect

Catena

journal homepage: www.elsevier.com/locate/catena

Evaluation of CFSR, TMPA 3B42 and ground-based rainfall data as input for hydrological models, in data-scarce regions: The upper Blue Nile Basin, Ethiopia

Abeyou W. Worqlul [a,b,*], Haw Yen [a], Amy S. Collick [c], Seifu A. Tilahun [d], Simon Langan [e], Tammo S. Steenhuis [b,d]

[a] Blackland Research and Extension Center, Texas A&M Agrilife Research, 720 East Blackland Road, Temple, TX 76502, USA
[b] Department of Biological and Environmental Engineering, Cornell University, Ithaca, NY, USA
[c] USDA-ARS, University Park, PA, USA
[d] School of Civil and Water Resource Engineering, Bahir Dar University, Bahir Dar, Ethiopia
[e] International Water Management Institute, Addis Ababa, Ethiopia

ARTICLE INFO

Article history:
Received 22 April 2016
Received in revised form 10 November 2016
Accepted 13 January 2017
Available online 24 January 2017

Keywords:
Ethiopia highlands
Monsoon climate
CFSR
TRMM
TMPA
HBV
PED

ABSTRACT

Accurate prediction of hydrological models requires accurate spatial and temporal distribution of rainfall. In developing countries, the network of observation stations for rainfall is sparse and unevenly distributed. Satellite-based products have the potential to overcome this shortcoming. The objective of this study is to compare the advantages and the limitation of commonly used high-resolution satellite rainfall products (Climate Forecast System Reanalysis (CFSR) and Tropical Rainfall Measuring Mission (TRMM) Multisatellite Precipitation Analysis (TMPA) 3B42 version 7) as input to hydrological models as compared to sparsely and densely populated network of rain gauges. We used two (semi-distributed) hydrological models that performed well in the Ethiopian highlands: Hydrologiska Byråns Vattenbalansavdelning (HBV) and Parameter Efficient Distributed (PED). The rainfall products were tested in two watersheds: Gilgel Abay with a relatively dense network of rain gauge stations and Main Beles with a relatively scarce network, both are located in the Upper Blue Nile Basin. The results indicated that TMPA 3B42 was not be able to capture the gauged rainfall temporal variation in both watersheds and was not tested further. CFSR over predicted the rainfall pattern slightly. Both the gauged and the CFSR reanalysis data were able to reproduce the streamflow well for both models and both watershed when calibrated separately to the discharge data. Using the calibrated model parameters of gauged rainfall dataset together with the CFSR rainfall, the stream discharge for the Gilgel Abay was reproduced well but the discharge of the Main Beles was captured poorly partly because of the poor accuracy of the gauged rainfall dataset with none of the rainfall stations located inside the watershed. HBV model performed slightly better than the PED model, but the parameter values of the PED could be identified with the features of the landscape.

Published by Elsevier B.V.

1. Introduction

Sound predictions of hydrological models need accurate spatial and temporal distribution of precipitation (Sharma et al., 2012). However, in developing countries, ground rainfall observation stations are often unevenly and sparsely distributed and this situation is unlikely to improve soon (Worqlul et al., 2014). According to the World Meteorological Organization (WMO, 1994) the minimum rainfall station network density for tropical regions are 600 to 900 km^2 per station for flat areas and 100 to 250 km^2 per station for mountainous regions. But, such a dense network in developing countries is generally not available (Conway, 2000; Taye and Willems, 2012). Recently, the availability of satellite rainfall products where there is limited or no conventional ground rainfall observation stations has attracted the interest of hydrologists (Collischonn et al., 2008; Hong et al., 2007; Yilmaz et al., 2005). Satellite rainfall estimates have the advantage of high temporal resolution and spatial coverage, even over mountainous regions and sparsely populated areas.

The Climate Forecast System Reanalysis (CFSR) and Tropical Rainfall Measuring Mission (TRMM) Multisatellite Precipitation Analysis (TMPA) 3B42 version 7, besides being widely used and freely available in Africa, both systems provide data with high spatial resolution, global coverage and high temporal resolution. TMPA 3B42 is available since 1998 in a spatial resolution of 0.25° by 0.25° grid (≈27 km at the equator) with a 3-hourly temporal resolution in a global belt extending from 50° N to 50° S. TMPA 3B42 version 6 provided valuable precipitation data in regions were gauged rainfall data is scarce such as Iran (Javanmard et al. (2010), for the Nzoia River Bain in Kenya (Ouma et

* Corresponding author at: Blackland Research and Extension Center, Texas A&M Agrilife Research, 720 East Blackland Road, Temple, TX 76502, USA.
E-mail address: aworqlul@brc.tamus.edu (A.W. Worqlul).

http://dx.doi.org/10.1016/j.catena.2017.01.019
0341-8162/Published by Elsevier B.V.

al., 2012), in the USA (Tian et al., 2007), and over Ethiopia (Dinku et al., 2007). In addition, the improved version 7 of TMPA 3B42RT which is near-real time and the research version 3B42 adjusted for monthly gauged rainfall has performed well in capturing the rainfall amounts and patterns (Chen et al., 2013; Moazami et al., 2014; Xue et al., 2013). According to Romilly and Gebremichael (2011), the near-real time version 3B42RT has performed well in capturing the five years averaged gauged rainfall in Ethiopia compared to Precipitation Estimation from Remotely Sensed Information Using Neural Networks (PERSIANN) and Climate Prediction Center morphing method (CMORPH) rainfall estimates. According to Chen et al. (2013) after comparing the real-time and research products with gauged rainfall data in the Mainland China the research version 3B42 performed much better than the real-time product 3B42RT. The CFSR global atmosphere data has a spatial resolution of approximately 38 km and the data is available since 1979 (Saha et al., 2010). Detailed information on TMPA and CFSR data can be found in (Huffman et al., 2007; Saha et al., 2010; Wang et al., 2011; Worqlul et al., 2014).

Validation of satellite rainfall products and reanalysis data can be achieved by direct comparison with the ground observation station network (Dinku et al., 2008; Bitew et al., 2012; Worqlul et al., 2014) or by their ability to predict streamflow using hydrological models (Bitew et al., 2012; Fuka et al., 2013). A variety of research work was implemented by different hydrologic models in the Ethiopian highlands, such as the Agricultural Non-Point Source Pollution (AGNPS) (Haregeweyn and Yohannes, 2003), Water Erosion Prediction Project (WEPP) (Zeleke, 2000) and the Soil and Water Assessment Tool (SWAT) (Setegn et al., 2008). However, few of the hydrological models applied in Ethiopia fall short to capture the saturation excess runoff mechanism. In some part of the country, it has been experimentally demonstrated that saturation excess runoff is the dominant mechanism of overland flow (Bayabil et al., 2010; Tilahun et al., 2013a; Tilahun et al., 2013b). Obviously applying a hydrological model with the underline assumption of infiltration-excess will not be able to provide methodically sound approaches to estimate saturation excess, so that the subsequent watershed-scale analysis may not be scientifically credible.

In this study, the Parameter Efficient Distributed (PED) (Steenhuis et al., 2009) and the Hydrologiska Byråns Vattenbalansavdelning (HBV) (Lindström et al., 1997) were applied to solve the potential issues of misinterpretation of hydrological processes. Both models incorporate saturation excess process into the computational schemes and they are not input data intensive. Both models could represent the runoff better in monsoon climates than infiltration excess runoff models for scales ranging from 100 ha basin to the whole Blue Nile basin (Tilahun et al., 2013a, 2013b; Steenhuis et al., 2014; Abdo et al., 2009; Wale et al., 2009).

The major goal of this study is to assess the suitability and performance of TMPA 3B42 and CFSR rainfall products in predicting runoff through hydrological model calibration. The limitations of state-of-the-art high-resolution satellite rainfall data were explored in Africa in simulating the discharge of two watersheds, Gilgel Abay and Main Beles, in the upper Blue Nile Basin, Ethiopia. Gilgel Abay basin has high-quality discharge data and a relatively well distributed network of ground rainfall observation station and Main Beles basin also has good quality discharge data, but a less well-endowed network of ground rainfall stations with a long period of daily data.

2. Methodology

2.1. Watershed description

The Gilgel Abay and Main Beles watershed are located in the Blue Nile Basin, in the western part of the Ethiopian highlands (Fig. 1). The Gilgel Abay watershed is located in the Tana basin, between 10°56′ to 11°58′N latitude and 36°44′ to 37°34′E longitudes. Gilgel Abay River is the source of Lake Tana; it originates from a small spring located near Gish Abay Mountain at elevation of 3000 m. Main Beles watershed is part of the Beles basin. Geographically it extends from 10°56′ to 12° N latitude and 35°12′ to 37° E longitude (Fig. 1). The watershed areas of the Gilgel Abay and Main Beles as extracted from the 30 m resolution Shuttle Radar Topographic Mission (SRTM) Digital Elevation Model (DEM) at their gauging sites were approximately 1650 km^2 and 3212 km^2, respectively. In Fig. 1, the location of meteorological stations and drainage pattern of the Gilgel Abay and Main Beles sub-basins are depicted.

Gilgel Abay and Main Beles basins have a complex topography with elevation ranging from 1890 to 3530 and 990 to 2725 m, respectively. The slope of the watersheds varies from 0 to 140%, with an average slope of 12% for Gilgel Abay and 14% for Main Beles basins. Approximately 50% of the watersheds have a slope <8%. Gilgel Abay receives annual average rainfall of 1860 mm while Main Beles receives an annual average of 1550 mm/year. The predominant wet season from June to September accounts for 70 to 90% of the annual rainfall (Kebede et al., 2006; Tarekegn and Tadege, 2006).

2.2. Climatological and discharge data

Climate data was collected from Ethiopian Meteorological Agency (EMA). Daily precipitation data was available from Dangila, Adet, Sekela and Enjibara stations starting from 1994 to 2006 and for Chagni and Pawi stations data was available from 1998 to 2006. Data required to estimate potential evaporation (maximum and minimum temperature, daily sunshine hour, maximum and minimum humidity and wind speed) were only available at the Dangila station from 1994 to 2006. Daily discharge data for Gilgel Abay and Main Beles at the outlet stations from 1994 to 2006 was obtained from Ethiopian Ministry of Water, Irrigation, and Energy.

2.3. Rainfall products

The two rainfall products evaluated were TMPA product 3B42 version 7 and CFSR. Dinku et al. (2010) and Huffman et al. (2007) describes that the TMPA-3B42 product is generated in four steps: (i) the Passive Microwave (PM) rainfall are calculated, (ii) Thermal Infrared (TIR) precipitation estimates are created using the calculated PM for calibration, (iii) PM and TIR estimates are combined, and (iv) the data is rescaled to monthly totals whereby gauge observations are used indirectly to adjust the satellite product (Huffman et al., 2007). The near-real time version 3B42RT is produced at the end of the third step; this data does not include gauge information (Huffman and Bolvin, 2013; Ouma et al., 2012). The product TMPA 3B42 has been available since 1998 with a spatial resolution of approximately 27 km at the equator and with a temporal resolution of 3 h.

The CFSR was designed and executed as a global, high-resolution coupled atmosphere–ocean–land surface–sea ice system to provide the best estimate of the state of these coupled domains for the study period (Saha et al., 2014). The new feature in CFSR includes: the first reanalysis system in which the guess fields are taken as the 6-h forecast from a coupled atmosphere–ocean climate system with an interactive sea ice component; and it assimilates satellite radiances and humidity values (Wang et al., 2011). The CFSR global atmosphere data has a spatial resolution of approximately 38 km and the data is available since 1979 (Saha et al., 2010). The daily gridded satellite rainfall estimation data of TMPA product (3B42) Version 7 was downloaded from the ftp server at ftp://disc2.nascom.nasa.gov/data/s4pa/TRMM_L3/TRMM_3B42 daily/and CFSR at http://rda.ucar.edu/datasets/ds094.1/. The CFSR data from the period 1994 to 2006 and TMPA 3B42 from 1998 to 2006 were considered in this study.

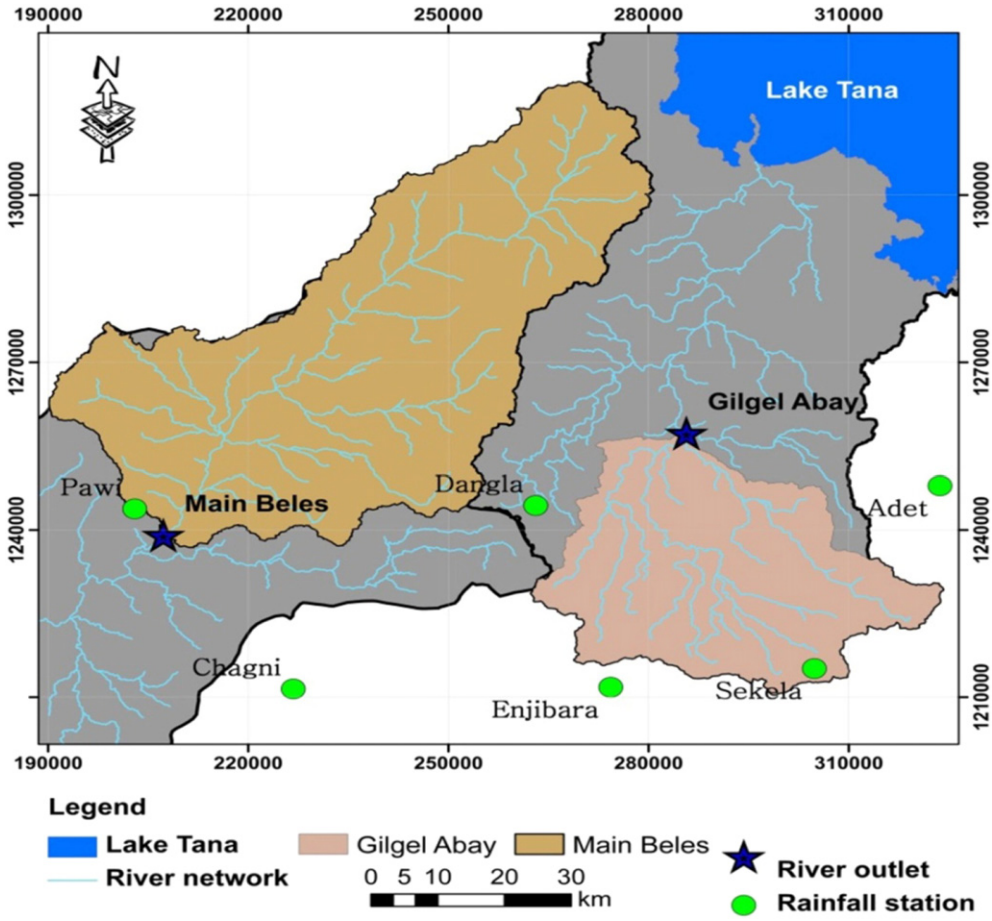

Fig. 1. Drainage pattern and meteorological station network of the Gilgel Abay and Main Beles basins.

2.4. Watershed models

Precipitation was converted to watershed discharge as described in Section 2.5 using the HBV and the PED models. Both models HBV and PED are considered as parsimonious models since they have a limited number of model parameters, making the calibration procedure less complicated and avoids the problem of over-parametrization (Whittaker et al., 2010) leading to a poor prediction accuracy. A brief description of the models is given below:

2.4.1. HBV model

The HBV (Hydrologiska Byråns Vattenbalansavdelning) model (Lindström et al., 1997) is a conceptual rainfall-runoff model for continuous daily simulation of catchment runoff. In HBV, the watershed is divided into sub-watersheds and further divided into elevation and land use zones. The model simulates daily runoff using daily rainfall, temperature, long-term average monthly potential evaporation, geographical information of the catchment which is sliced elevation crossed with land use and observed runoff data for calibration. The general water balance is described in Eq. (1):

$$P-E-Q=\frac{d}{dt}[SP+SM+UZ+LZ+L] \quad (1)$$

where P is the precipitation, E is evapotranspiration, Q is runoff, SP is snow pack, SM is soil moisture, UZ is runoff contribution from upper reservoir, LZ is runoff contribution from lower reservoir, and L is the lake volume.

The model consists of subroutines for precipitation, soil moisture, response, transformation functions and simple routing procedure. The soil moisture accounting routine is based on three parameters: Beta, FC and LP. Beta controls the contribution to the response function from each millimeter of rainfall. FC is the maximum soil moisture storage. As the soil moisture exceeds the limit for potential evaporation (LP), water will evaporate at a potential rate. The response routine is described by an upper non-linear reservoir and a linear lower response routine connected with the upper box with percolation (PERC). Khq and K4 are recession coefficient parameters for the upper and lower reservoir, respectively. The non-linearity of the upper reservoir is controlled by the parameter Alpha. The higher Alpha value will higher the peaks and a quicker recession (SMHI, 2006). A complete description of the

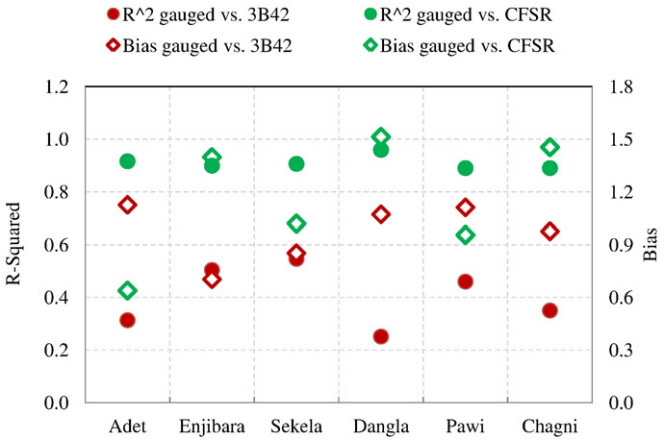

Fig. 2. Long-term average monthly R-square and Bias of TMPA 3B42 and CFSR rainfall estimate vs. ground rainfall observation stations within the rainfall product grid box.

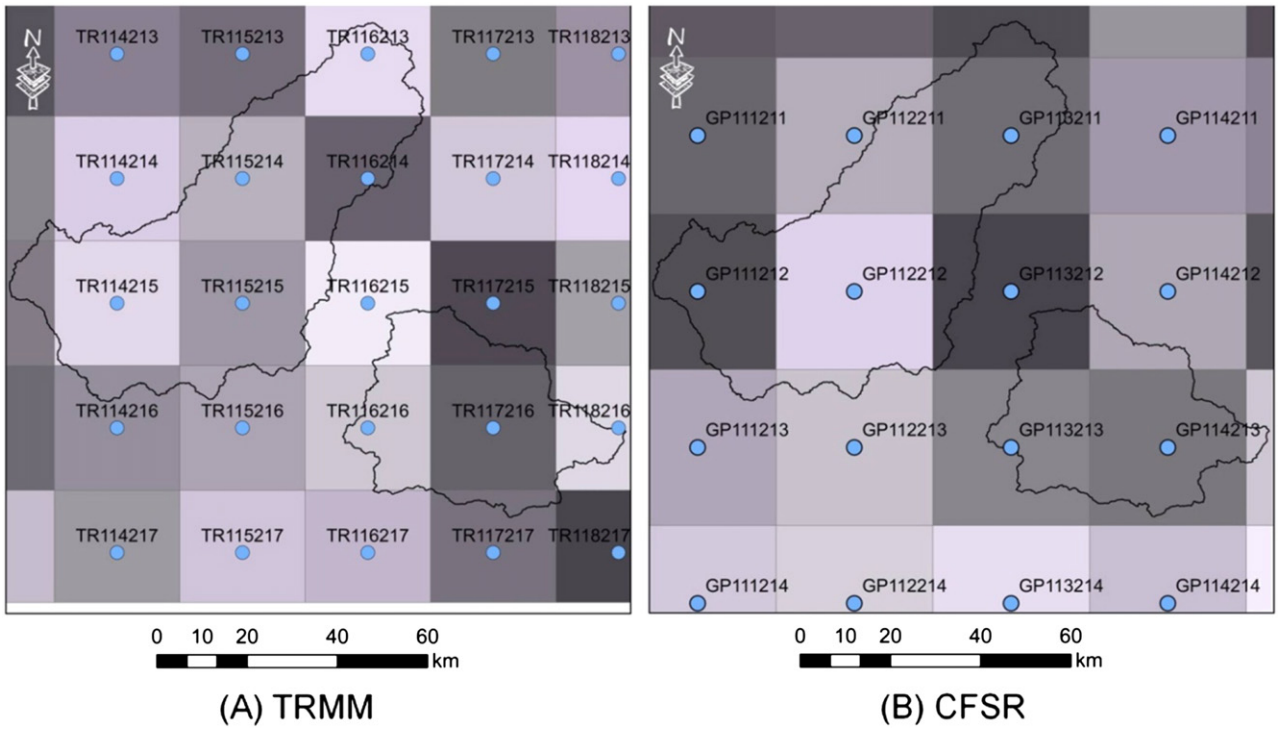

Fig. 3. Rainfall observation grid of (A) TMPA 3B42 and (B) CFSR for Gilgel Abay and Main Beles basins. Grid size is approximately 27 km and 38 km for 3B42 and CFSR, respectively.

HBV model can be found in Lindström et al. (1997), SMHI (2006) and Wale et al. (2009) among others. Inputs for HBV long-term monthly potential evaporation was estimated by the Penman-combination equation using Dangila meteorological station. A digital elevation model (DEM) of 30 m resolution from SRTM DEM (Jarvis et al., 2008) was used to extract the drainage area of the watersheds and to divide each watershed into three different sub-basins and elevations zones. Land use data was collected from Ethiopia Ministry of Water, Irrigation, and Energy.

2.4.2. PED model

The PED (Parameter Efficient Distributed) model (Steenhuis et al., 2009) is a conceptual semi-distributed rainfall-runoff model for continuous daily simulation of catchment runoff. In PED, the watershed is subdivided into three sub-regions distinguished as the bottom lands that are potentially saturated in the rainy monsoon phase, degraded hillslope/exposed rock with little or no soil cover and permeable hillslopes (infiltration zones). Various portions of the watershed become hydrologically active when threshold moisture content is exceeded (Steenhuis et al., 2013). The permeable hillslopes/infiltration zones contribute to the rapid subsurface flow (called interflow) characterized by flow decreasing as a linear function of time, and baseflow is characterized by an exponentially decreasing flow in time (Steenhuis et al. (2013). Overland flow is generated from saturated areas in the relatively flatter areas in the landscape and areas where bedrock is exposed Steenhuis et al. (2009). For each of the three regions, the water

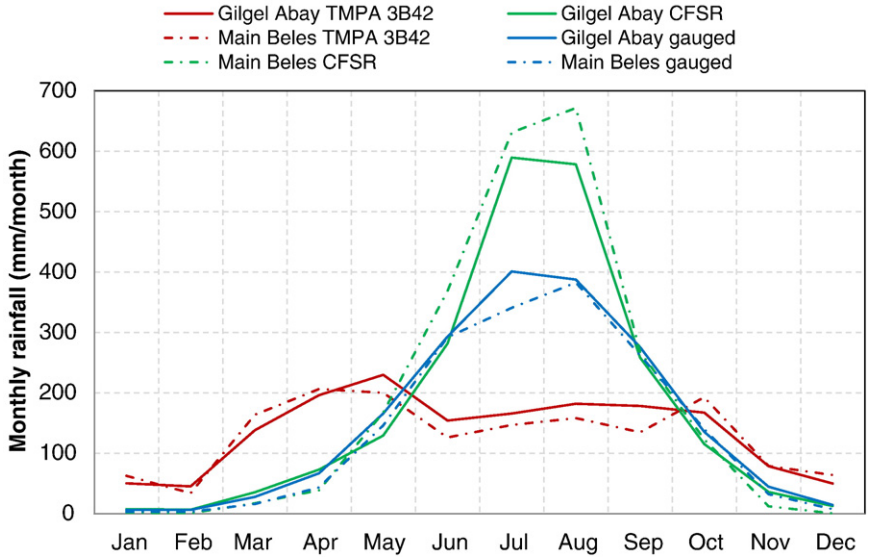

Fig. 4. Long-term monthly average areal rainfall of gauged rainfall, CFSR data (from 1994 to 2003) and TMPA 3B42 (from 1998 to 2003) for Gilgel Abay and Main Beles basins.

Table 1
Coefficient of determination (R^2) areal gauged and rainfall products over Gilgel Abay and Main Beles basins.

Basins		Main Beles			Gilgel Abay		
		TMPA	CFSR	Gauged	TMPA	CFSR	Gauged
Main Beles	TMPA	1.00	–	–	–	–	–
	CFSR	0.10	1.00	–	–	–	–
	Gauged	0.15	0.93	1.00	–	–	–
Gilgel Abay	TMPA	0.87	0.26	0.37	1.00	–	–
	CFSR	0.11	0.99	0.90	0.26	1.00	–
	Gauged	0.16	0.94	0.99	0.38	0.93	1.00

balance calculation is based on the procedure proposed by Thornthwaite and Mather (1955). The general water balance equation for the sub-regions is described in Eq. (2):

$$S_t = S_{t-\Delta t} + (P - AET - R - Perc)\Delta t \quad (2)$$

where S_t is water stored in the topmost layer, $S_{t-\Delta t}$ is the previous time step storage (mm), P is precipitation (mm day^{-1}), AET is the actual evapotranspiration, R is the saturation excess runoff (mm day^{-1}), Perc is the percolation to the subsoil (mm day^{-1}), and Δt is the time step (day).

The model simulates the daily runoff using daily rainfall, potential evaporation and daily runoff data for calibration. Inputs for PED: potential evaporation was estimated by the Penman-combination equation. Landscape parameters for the model, the relative area of three regions was used as a model calibration parameter with their respective maximum soil moisture storage capacity. Subsurface flow is simulated using a linear reservoir with a half-life ($t_{1/2}$) and interflow employing a zero order reservoir calibration parameter τ^* is the duration of the period after a single rainstorm until interflow ceases. A complete description of the PED model can be found in Steenhuis et al. (2009), Tesemma et al. (2010), Tilahun et al. (2013b) and Caballero et al. (2013).

2.5. Methods

The two precipitation products (3B42 and CFSR) were evaluated by comparing the rainfall amounts with the gauged rainfall data and by using the precipitation data as input to the HBV and PED models to predict the observed discharge of Gilgel Abay and Main Beles sub-watersheds.

2.5.1. Comparing rainfall products with gauged data

The rainfall products were compared in two ways.

1. The monthly gauged rainfall was compared with the monthly rainfall amounts of 3B42 and CFSR products for the grid box in which the stations were located. The performance of 3B42 and CFSR data in capturing the gauged rainfall were evaluated with a performance statistics.
2. Monthly average aerial precipitation for watersheds for the two rainfall products and the gauged rainfall were compared. Areal rainfall of gauged and rainfall products were estimated by using inverse distance interpolation. The performance of 3B42 and CFSR data were tested with coefficient of determination and percent bias were calculated.

Table 2
Optimized model parameter set of PED and model performance for gauged rainfall and CFSR data for Gilgel Abay and Main Beles.

Description		Gilgel Abay		Main Beles	
		Gauged rainfall	CFSR	Gauged rainfall	CFSR
Fraction of saturated area (%)		0.07	0.06	0.02	0.02
Fraction of degraded area (%)		0.05	0.05	0.05	0.02
Fraction of hillside area (%)		0.86	0.57	0.73	0.35
$t_{1/2}$ (days)		45	45	18	20
τ^* (days)		40	40	46	66
Calibration period (1994 to 2003)	PBIAS (%)	10	7.6	-8.0	4.9
	NSE	0.74	0.73	0.61	0.63
	R^2	0.75	0.74	0.63	0.65
Validation period (2004 to 2006)	PBIAS (%)	−9.2	−5.9	−9.0	6.2
	NSE	0.65	0.63	0.68	0.66
	R^2	0.76	0.68	0.69	0.72

2.5.2. Comparing rainfall products as input to a hydrological model

Two types of analysis are performed: First both PED and HBV model best-fit parameters were determined for the rainfall product and gauged rainfall datasets separately. Then the gauged rainfall calibrated model was used to predict the observed flow using the rainfall products as input.

Prior to model calibration, model parameter space in terms of minimum and maximum bounds were specified to represent the watershed conditions based on literature and local knowledge. For initialization of HBV, the optimized model parameter sets of Rientjes et al. (2011) and for the PED model that of Steenhuis et al. (2009) and Tilahun et al. (2013b) were used. The HBV model in Rientjes et al. (2011) was calibrated by an automatic procedure using a Monte Carlo computation procedure. For PED model, a semi-automatic procedure was implemented by increasing the most sensitive parameter (i.e., fractional hillslope area) and then varying the other parameters systematically near the optimum) until the optimum solution was found. The models were calibrated for gauged rainfall and CFSR data. The calibration for the CFSR rainfall product and the gauged network were for the period

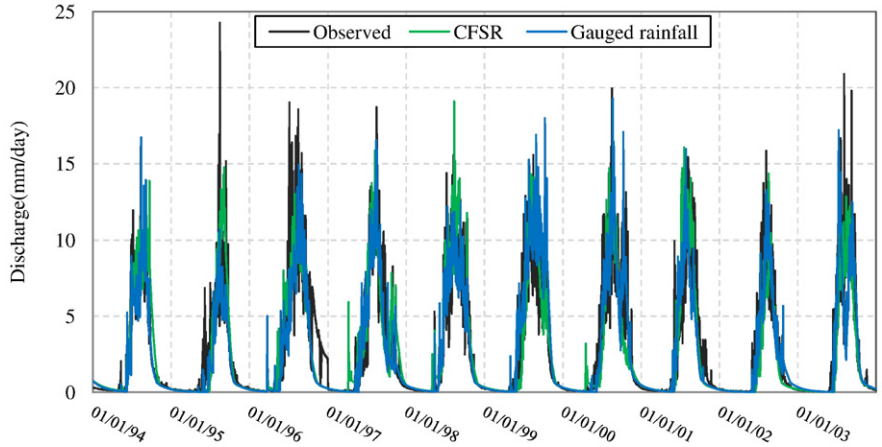

Fig. 5. Simulated flow of PED model by gauged rainfall and CFSR data plotted with observed flow for Gilgel Abay basin.

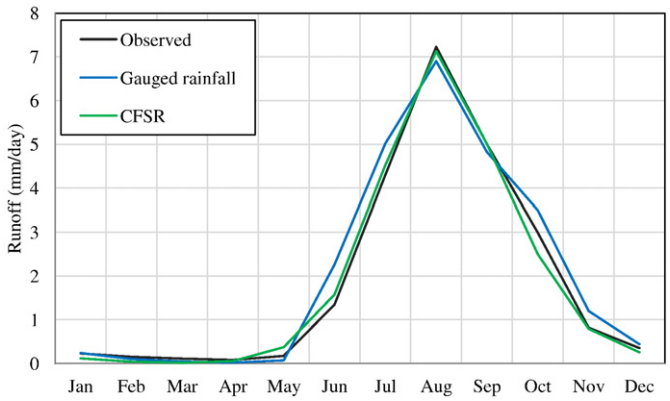

Fig. 6. Comparison of long-term average monthly Gilgel Abay observed flow and PED simulation for gauged rainfall and CFSR (from 1994 to 2003).

Table 3
Optimized model parameter set of HBV model and its performance for gauged rainfall and CFSR data.

Description		Gilgel Abay		Main Beles	
		Gauged rainfall	CFSR	Gauged rainfall	CFSR
Alpha		0.50	0.50	0.80	0.50
Beta		1.00	1.00	1.30	1.00
FC		245	1200	650	1400
LP		0.99	0.99	0.70	0.40
PERC		1.30	1.08	0.70	0.60
K4		0.04	0.04	0.002	0.002
Khq		0.10	0.08	0.13	0.08
Calibration period (1994 to 2003)	PBIAS (%)	3.02	6.81	-3.12	2.82
	NSE	0.78	0.72	0.63	0.62
	R^2	0.79	0.73	0.65	0.63
Validation period (2004 to 2006)	PBIAS (%)	10.0	0.19	9.2	9.6
	NSE	0.71	0.62	0.61	0.60
	R^2	0.81	0.68	0.63	0.61

from 1994 to 2003 and for TMPA 3B42 rainfall product was from 1998 to 2003. In all cases, the calibrated models were validated from 2004 to 2006.

The model performance was evaluated by multiple objective functions such as the Nash-Sutcliffe Efficiency (NSE, Nash and Sutcliffe, 1970), percent bias (PBIAS), and coefficient of determination (R^2). NSE is a normalized statistic that determines the relative magnitude of the residual variance compared to the measured observed flow variance. NSE ranges from negative infinite to one. Generally, NSE value between 0.6 and 0.8 indicates fair to good performance, and a model is said to be very good when NSE is above 0.8 (Moriasi et al., 2007). PBIAS is the relative difference between the observed and simulated flows. PBIAS measures the tendency of the average simulated flow to be larger or smaller than the observed flow (Gupta et al., 1999). R^2 is used to evaluate the goodness of fit of the relations. R^2 examines the degree of linear association between the observed and simulated flows.

Finally, the calibration was followed by sensitivity analysis of the model parameters. Sensitivity analysis will help as to indicate the level of variability of the simulated flow or output for the input model parameters. The sensitivity analysis was done to identify and rank the level of sensitivity of the parameters in the respective watersheds. In this study, sensitivity analysis was done by a local sensitivity analysis technique. In a local sensitivity analysis, a single model parameter is simulated multiple times for the model parameter space keeping the other model parameter at a nominal value (Muleta and Nicklow, 2005; Passuello et al., 2012; Saltelli et al., 1999).

3. Results and discussion

3.1. Comparison of gauged rainfall with 3B42 and CFSR precipitation products

The monthly rainfall data of the gauged rainfall was compared with the rainfall of 3B42 and CFSR products for the grids in which the stations were located. In Fig. 2, the statistics (R^2 and Bias) of the point to grid comparison is shown. The grid network for both rainfall products is presented in Fig. 3. The CFSR data was more alike ($R^2 > 89\%$) to the gauged rainfall than the 3B42 ($R^2 < 55\%$, Fig. 2). The bias calculated as a ratio of the mean annual rainfall product to the gauged rainfall data was approximately the same for 3B42 and CFSR data ranging between 0.70 and 1.13 and 0.64 to 1.51 (Fig. 2).

Similarly, we compared the monthly average aerial precipitation of both watersheds (calculated by inverse distance interpolation and averaged from 1994 to 2006 for CSRF and 1998 to 2006 for 3B42, Fig. 4). The CFSR and gauged rainfall are more similar ($R^2 > 93\%$, Table 1) than the 3B42 ($R^2 = 38\%$ and 15% for Gilgel Abay and Main Beles, respectively). The bias calculated as a ratio of annual mean of rainfall products to the annual gauged rainfall was 0.9 for 3B42 and 1.20 for CFSR data in Gilgel Abay and 0.94 for 3B42 and 1.37 for CFSR in Main Beles.

TMPA 3B42 average annual areal rainfall volume under-predicted the gauged rainfall by 10% and 6% for Gilgel Abay and Main Beles, respectively. CFSR data over-predicted the gauged rainfall by 20% and 37%, respectively. The gauged rainfall indicated that 75% of the rainfall occurs during the rainy season from June through September compared

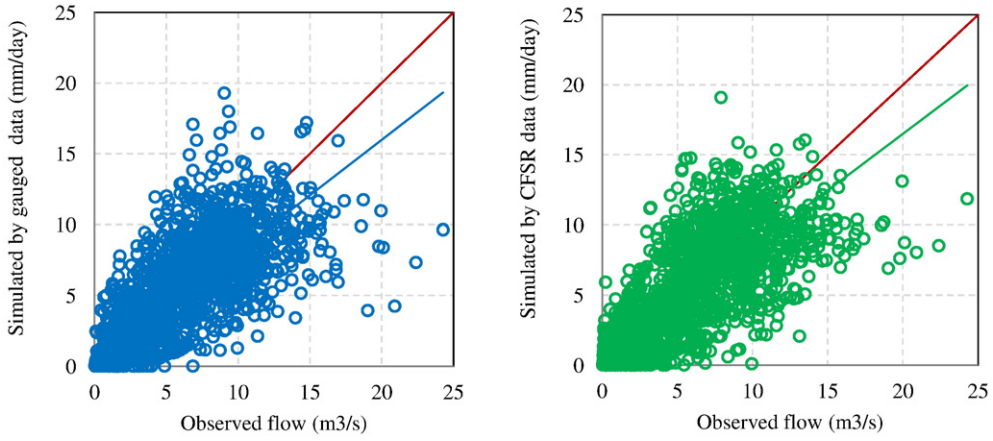

Fig. 7. Correlation between observed flow and simulated flow for the calibration period using (a) gauged rainfall and (b) CFSR data for the Gilgel Abay Basin using PED model.

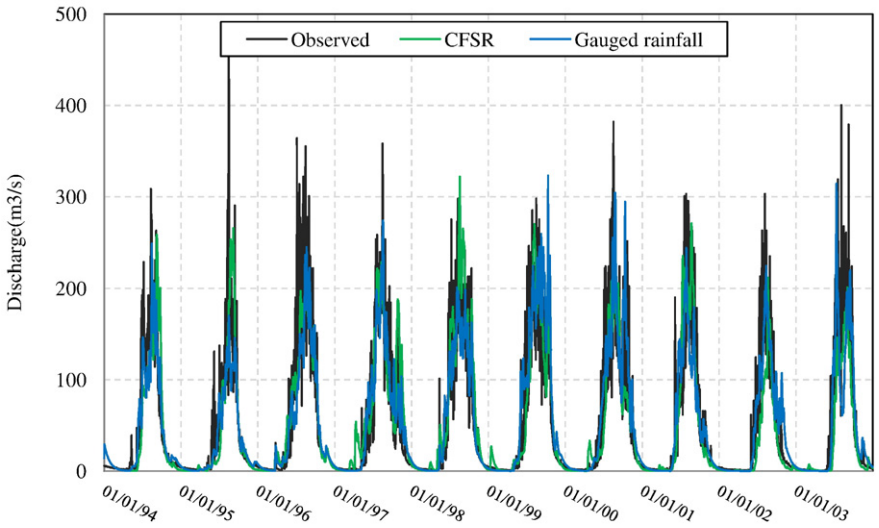

Fig. 8. Simulated flow of HBV model by gauged rainfall and CFSR data plotted with observed flow for Gilgel Abay basin (1994–2003).

to 80% for CFSR and only 39% for 3B42. Thus, the TMPA 3B42 satellite rainfall data does not capture the temporal variation of rainfall well for either point to grid or areal comparison. The poor seasonal rainfall predictions will cause the misrepresentation of watershed discharge, with nearly 82% and 83% of annual discharge occurs between June through September for Gilgel Abay and Main Beles.

In this study, the TMPA 3B42 rainfall product performed poorly while it has been shown to perform well in some part of the world (Javanmard et al., 2010; Moazami et al., 2014; Ochoa et al., 2014; Ouma et al., 2012; Tian et al., 2007). There is a relatively simple explanation why the TMPA 3B42 does not perform well in our study and that of Dinku et al. (2008) and Haile et al. (2013). According to Haile et al. (2013), while bias correction was done by TMPA, the gauged rainfall data of the Blue Nile Basin was not made available. The bias of the bear-real-time 3B42RT was corrected by the Global Precipitation Climatology Centre (GPCC) data (Zulkafli et al., 2014). The distribution of the GPCC and the number of station per grid is scarce in Central and East part of Africa. There is only one GPCC station in Ethiopia, and it is outside the Blue Nile Basin. Therefore, further adjustment has to be done to use TMPA 3B42 rainfall products in the Blue Nile Basin. Since TMPA 3B42 performed poorly in capturing the gauged rainfall pattern, only CFSR and gauged rainfall data were used as an input to the watershed models HBV-IHMS and PED for daily discharge simulation of Gilgel Abay and Main Beles watersheds.

3.2. Simulated discharge using PED and HBV models

In this section, we will first test how well both the CFSR and gauged rainfall data can predict the discharge by calibrating the PED and HBV model separately. Then assuming that the rain gauge data provides the best input data for the models, we will test how well the CFSR can predict the observed streamflow as input to the gauged rainfall calibrated parameter.

3.2.1. Simulation of stream discharge with PED model

The calibrated PED model using gauged rainfall or CFSR rainfall captured the observed daily stream flow reasonably well for both the calibration and validation periods. For the calibration period of Gilgel Abay, the gauged rainfall indicated NSE of 0.74 and CFSR data has NSE of 0.73. For Main Beles, for the calibration period, the gauged rainfall indicated NSE value of 0.61 while CFSR indicated 0.63; see Fig. 5 and Table 2. For both basins, as demonstrated in Fig. 6 in which the average monthly values are depicted and Table 2, the gauged rainfall gave slightly better result than the CFSR data (Fig. 7a and b). For the daily values, the same trend was observed in which, the regression coefficient indicated that during the validation period of the Gilgel Abay basin the gauged rainfall captured 76% of the observed runoff variation and CFSR captured 68% of the flow variation (Table 2).

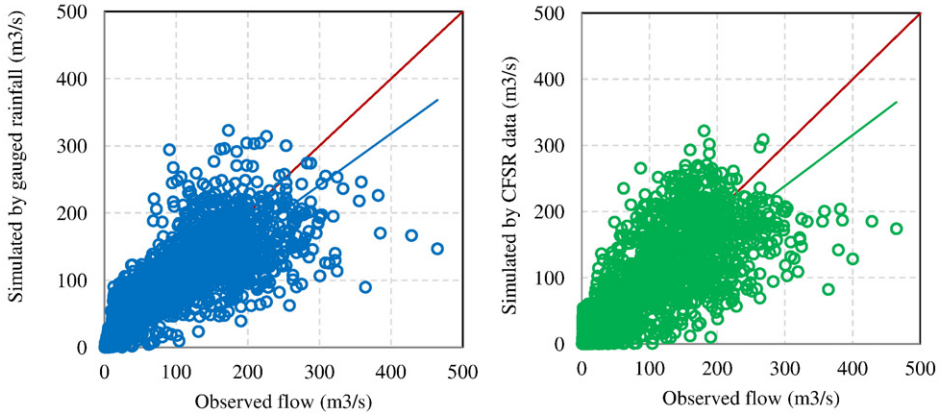

Fig. 9. Correlation between observed flow and simulated flow for the calibration period using (a) gauged rainfall and (b) CFSR data for the Gilgel Abay Basin using HBV model.

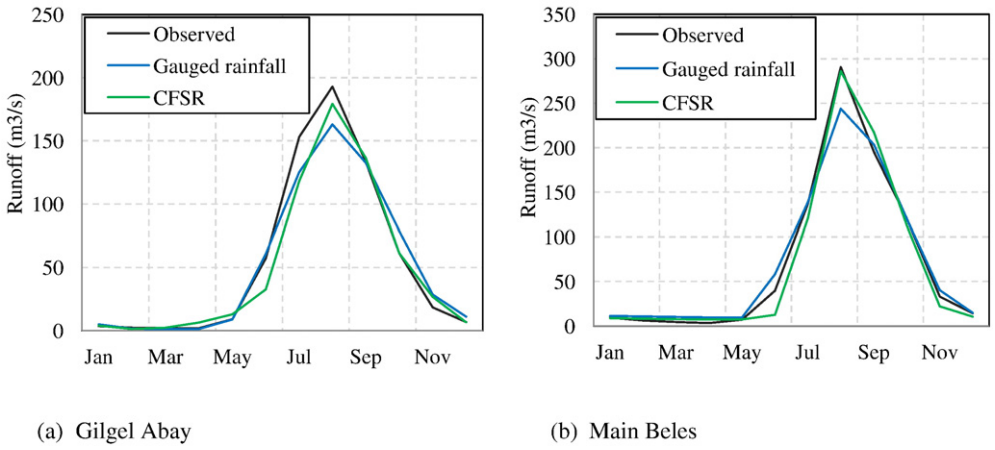

Fig. 10. Comparison of long-term average monthly-observed flow and HBV simulation for gauged rainfall and CFSR rainfall estimate of (a) Gilgel Abay and (b) Main Beles basins.

Table 2 also lists the optimized PED model parameter sets for the gauged and CFSR data for Gilgel Abay and Main Beles basins. The calibrated model parameters for the subsurface flow represented by the half-life ($t_{1/2}$) and interflow calibration parameter τ^* for the different rainfall input data were almost the same for all simulations as expected and consistent with values used in simulation of Anjeni and Blue Nile Basins (Tilahun et al., 2013a). The fractional regions contributing to rapid subsurface and overland flow have different values for the gauged rainfall and CFSR rainfall simulations. The total contributing area for the gauged rainfall adds up to 98% for Gilgel Abay and 80% for Main Beles. This is also consistent with earlier studies of PED simulation for a wide scale of watershed study areas by Tilahun et al. (2013b) which indicated that the fractional area's for a 180,000 km^2 Blue Nile Basin adds up to 100% while the smaller watershed of <5 km^2 area was in the order of 60%. Therefore, for a mid-range watershed area in a range of 1000 km^2 the fraction area up to 80 to 97% would be realistic. Using CFSR the fractional area adds up to 68% for the Gilgel Abay and 39% for the Main Beles indicating that the CFSR over predicts the actual rainfall in the basin and is consistent with the results in Section 3.1.

3.2.2. Simulation of stream discharge with HBV model

The semi-distributed HBV model has seven parameters controlling the total volume and shape of the hydrograph. The optimized model parameter sets of both watersheds and simulated discharge versus observed runoff for gauged rainfall and CFSR data of Gilgel Abay is shown in Table 3 and Fig. 8.

The simulated flow for the calibration period using the gauged rainfall and CFSR showed a fair to good performance with a daily NSE value of 0.78 and 0.72 for Gilgel Abay and 0.63 and 0.62 for Main Beles, respectively, and with acceptable R^2 and PBIAS (Moriasi et al., 2007) (Table 3, Fig. 9a and b). The simulation for both gauged rainfall and CFSR data captured the baseflow as well as the rising and recession limb adequately. Fig. 10 depicts the long-term monthly average observed flow and simulated flow for gauged rainfall and CFSR data of Gilgel Abay and Main Beles basins.

Table 4
Result of CFSR data flow simulation using gauged rainfall calibrated model parameters for Gilgel Abay and Main Beles watersheds.

Model performance		Gilgel Abay		Main Beles	
		HBV	PED	HBV	PED
CFSR cross validation	PBIAS (%)	−25.2	−18.3	−49.2	−41.9
	NSE	0.50	0.42	0.15	0.14
	R^2	0.74	0.72	0.58	0.60

The peak flow is better captured by the CFSR data than the gauged rainfall although both simulations underestimate very high single peaks that are commonly caused by extreme high rainfall events. For the study period, in the Gilgel Abay watershed, there were 505 days with observed flow above 200 m^3/s, the simulation by the CFSR rainfall product captured 340 events and the gauged rainfall captured 235 events. The optimized model parameters of the gauged rainfall and CFSR data have similar values except for Field capacity (FC, see Table 3). The FC of the calibrated model using CFSR data was significantly greater than the FC value of model calibrated by gauged rainfall (1200 and 245 mm for Gilgel Abay and 1400 and 650 mm for Main Beles, respectively). The FC value for the simulation with the CFSR product represents greater quantities of water retained in the soil that is released afterwards by evapotranspiration and baseflow compared to the gauged flow simulation. It is the model's way to account for a greater amount of rainfall of CFSR data compared to the gauged rainfall. The optimized model parameter set was tested for independent data from 2004 to 2006 and according to Moriasi et al. (2007) the result was acceptable for both gauged rainfall and CFSR data for both watersheds.

3.2.3. Validation of CFSR rainfall estimate by gauged rainfall calibrated and validated parameters

The optimized model parameter sets of the gauged rainfall were used to evaluate the performance of CFSR data in predicting the observed flow of the study watersheds. This was achieved by rerunning the calibrated and validated gauged rainfall model with CFSR rainfall product as input while keeping the optimized gauged rainfall parameters constant. The performance of the simulated flow captured the observed flow pattern with R^2 between 0.58 and 0.74 for both watersheds and both models, but significant volume difference was observed between the observed and simulated flows (Table 4). For Gilgel Abay, NSE value of 0.42 for PED and 0.50 for HBV was observed but for Main Beles, both models did not perform well, the NSE was <0.2 for both models. The cross-validation indicated that CFSR data performed better in Gilgel Abay, this is partly because the gauged rainfall data was much more accurate in the Gilgel Abay watershed than Main Beles. The cross-validation indicated the need for CFSR rainfall product to be directly calibrated to the streamflow. In areas with poor coverage of gauged rainfall data the calibrated model parameters could not reasonably represent the watershed hydrology.

4. Conclusion

In this study, the performance of commonly used high-resolution rainfall products Climate Forecast System Reanalysis (CFSR) and Tropical Rainfall Measuring Mission (TRMM) Multisatellite Precipitation Analysis (TMPA) 3B42 version were compared to in situ measurements.

In addition, CFSR and gauged rainfall data performance were evaluated by their prediction capacity of observed flow as input to a semi-distributed hydrological models HBV and PED through parameter calibration in Gilgel Abay and Main Beles basins, Ethiopia. The CFSR data was also used as input to the gauged rainfall calibrated hydrological model to test the performance of calibrated parameters on a relatively dense and sparse rainfall gauging station network.

The results of comparisons between CFSR and 3B42 data with the gauged rainfall indicated that CFSR data captured the pattern and volume of gauged rainfall well while 3B42 did not. According to the predefined statistical standards (Moriasi et al., 2007), the gauged rainfall has performed well in capturing the observed flow for both calibration and validation periods with a fair to good NSE and on average the simulation has explained approximately 70% of the observed flow variation through model calibration for both models. Rainfall estimate from the CFSR has also captured the observed flow through model calibration with a fair to good NSE and on average the CFSR runoff simulation has captured approximately 69% of the variation of the observed flow for both models. PED and HBV models responded for the excess rainfall of CFSR rainfall data. In HBV model, the maximum soil moisture storage parameter (FC) was too large indicating a deeper hydraulically active soil increasing the storage capacity of the soil. In PED model, the fractional contributing area for CFSR rainfall adds up to 68% for Gilgel Abay and 39% for Main Beles, while the fractional contribution area for the gauged rainfall were 98% and 80% for Gilgel Abay and Main Beles, respectively.

The TMPA 3B42 data was not tested to simulate the observed flow since it was unable to capture the gauged rainfall amount and pattern. We suggest further calibration of the TMPA 3B42 for the Blue Nile area before the data is used for any application. The performance of CFSR data cross-validated with the calibrated and validated model parameter sets of gauged rainfall captured the pattern of observed flow well but with a higher volume error. The cross-validation indicated CFSR data performed better for the Gilgel Abay compared to the Main Beles watershed in capturing the observed flow. This was caused by the gauged rainfall data quality of Gilgel Abay which is more representative of the area than in the Main Beles.

Although only one of the stations was inside in Gilgel Abay watershed the performance of the gauged rainfall in capturing the observed runoff was better than both CFSR and TMPA 3B42 rainfall products for calibration as well as validation periods. However, in Main Beles where there is no rainfall gauging station inside the watershed, CFSR data captured the observed flow better than gauged rainfall. This indicates that gauged rainfall has its merit, but for remote regions with few or no observation stations in the Blue Nile area, CFSR rainfall estimate can be used to complement gauged rainfall data scarcity with some caution of the model parameters. The fractional saturated and degraded area of the PED model can be validated through satellite imagery by supervised land use classification. The simulation by the CFSR data for both HBV and PED models was able to capture the peak flows better than the runoff simulation by the gauged rainfall. Therefore, the CFSR data might be more suitable to predict extreme events when using either PED or HBV models.

Acknowledgments

This research was supported by a graduate student fellowship for the senior author by the Norman E. Borlaug Leadership Enhancement in Agriculture Program (Award Number 016258-68) funded by the USAID and the International Water Management Institute (SAP REF: 45-16214). We would like to acknowledge the Ethiopian Ministry of Water, Irrigation and Energy and National Meteorological Agency of Ethiopia for providing daily river flow and meteorological data for multiple stations free of charge.

The editor and the two anonymous reviewers gratefully acknowledged for their valuable comments on our manuscript.

References

Abdo, K., Fiseha, B., Rientjes, T., Gieske, A., Haile, A., 2009. Assessment of climate change impacts on the hydrology of Gilgel Abay catchment in Lake Tana basin, Ethiopia. Hydrol. Process. 23 (26), 3661–3669.
Bayabil, H.K., Tilahun, S.A., Collick, A.S., Yitaferu, B., Steenhuis, T.S., 2010. Are runoff processes ecologically or topographically driven in the (sub) humid Ethiopian highlands? The case of the Maybar watershed. Ecohydrology 3, 457–466.
Bitew, M.M., Gebremichael, M., Ghebremichael, L.T., Bayissa, Y.A., 2012. Evaluation of high-resolution satellite rainfall products through streamflow simulation in a hydrological modeling of a small mountainous watershed in Ethiopia. J. Hydrometeorol. 13, 338–350.
Caballero, L.A., Easton, Z.M., Richards, B.K., Steenhuis, T.S., 2013. Evaluating the bio-hydrological impact of a cloud forest in Central America using a semi-distributed water balance model. Journal of Hydrology and Hydromechanics 61 (9-20b).
Chen, S., et al., 2013. Similarity and difference of the two successive V6 and V7 TRMM multisatellite precipitation analysis performance over China. J. Geophys. Res. Atmos. 118, 13,060–13,074.
Collischonn, B., Collischonn, W., Tucci, C.E.M., 2008. Daily hydrological modeling in the Amazon basin using TRMM rainfall estimates. J. Hydrol. 360, 207–216.
Conway, D., 2000. The climate and hydrology of the Upper Blue Nile River. Geogr. J. 166, 49–62.
Dinku, T., Chidzambwa, S., Ceccato, P., Connor, S., Ropelewski, C., 2008. Validation of high-resolution satellite rainfall products over complex terrain. Int. J. Remote Sens. 29, 4097–4110.
Dinku, T., Connor, S.J., Ceccato, P., 2010. Comparison of CMORPH and TRMM-3B42 over mountainous regions of Africa and South America. Satellite Rainfall Applications for Surface Hydrology. Springer, pp. 193–204.
Dinku, T., et al., 2007. Validation of satellite rainfall products over East Africa's complex topography. Int. J. Remote Sens. 28 (7), 1503–1526.
Fuka, D.R., et al., 2013. Using the climate forecast system reanalysis as weather input data for watershed models. Hydrol. Process.
Gupta, H.V., Sorooshian, S., Yapo, P.O., 1999. Status of automatic calibration for hydrologic models: comparison with multilevel expert calibration. J. Hydrol. Eng. 4, 135–143.
Haile, A.T., Habib, E., Elsaadani, M., Rientjes, T., 2013. Inter-comparison of satellite rainfall products for representing rainfall diurnal cycle over the Nile basin. Int. J. Appl. Earth Obs. Geoinf. 21, 230–240.
Haregeweyn, N., Yohannes, F., 2003. Testing and evaluation of the agricultural non-point source pollution model (AGNPS) on Augucho catchment, western Hararghe, Ethiopia. Agric. Ecosyst. Environ. 99 (1), 201–212.
Hong, Y., Adler, R.F., Negri, A., Huffman, G.J., 2007. Flood and landslide applications of near real-time satellite rainfall products. Nat. Hazards 43, 285–294.
Huffman, G.J., Bolvin, D.T., 2013. TRMM and Other Data Precipitation Data Set Documentation. NASA, Greenbelt, USA, pp. 1–40.
Huffman, G.J., et al., 2007. The TRMM multisatellite precipitation analysis (TMPA): quasi-global, multiyear, combined-sensor precipitation estimates at fine scales. J. Hydrometeorol. 8, 38–55.
Jarvis, A., Reuter, H.I., Nelson, A., Guevara, E., 2008. Hole-filled Seamless SRTM Data V4. International Centre for Tropical Agriculture (CIAT).
Javanmard, S., Yatagai, A., Nodzu, M., BodaghJamali, J., Kawamoto, H., 2010. Comparing high-resolution gridded precipitation data with satellite rainfall estimates of TRMM_3B42 over Iran. Adv. Geosci. 25, 119–125.
Kebede, S., Travi, Y., Alemayehu, T., Marc, V., 2006. Water balance of Lake Tana and its sensitivity to fluctuations in rainfall, Blue Nile basin, Ethiopia. J. Hydrol. 316, 233–247.
Lindström, G., Johansson, B., Persson, M., Gardelin, M., Bergström, S., 1997. Development and test of the distributed HBV-96 hydrological model. J. Hydrol. 201, 272–288.
Moazami, S., Golian, S., Hong, Y., Sheng, C., Kavianpour, M.R., 2014. Comprehensive evaluation of four high-resolution satellite precipitation products over diverse climate conditions in Iran. Hydrol. Sci. J.
Moriasi, D., et al., 2007. Model evaluation guidelines for systematic quantification of accuracy in watershed simulations. Trans. ASABE 50, 885–900.
Muleta, M.K., Nicklow, J.W., 2005. Sensitivity and uncertainty analysis coupled with automatic calibration for a distributed watershed model. J. Hydrol. 306, 127–145.
Nash, J., Sutcliffe, J., 1970. River flow forecasting through conceptual models part I—a discussion of principles. J. Hydrol. 10, 282–290.
Ochoa, A., Pineda, L., Crespo, P., Willems, P., 2014. Evaluation of TRMM 3B42 Precipitation Estimates and WRF Retrospective Precipitation Simulation Over the Pacific–Andean Region of Ecuador and Peru.
Ouma, Y.O., Owiti, T., Kipkorir, E., Kibiiy, J., Tateishi, R., 2012. Multitemporal comparative analysis of TRMM-3B42 satellite-estimated rainfall with surface gauge data at basin scales: daily, decadal and monthly evaluations. Int. J. Remote Sens. 33, 7662–7684.
Passuello, A., Cadiach, O., Perez, Y., Schuhmacher, M., 2012. A spatial multicriteria decision-making tool to define the best agricultural areas for sewage sludge amendment. Environ. Int. 38, 1–9.
Rientjes, T., Perera, B., Haile, A., Reggiani, P., Muthuwatta, L., 2011. Regionalisation for lake level simulation—the case of Lake Tana in the Upper Blue Nile, Ethiopia. Hydrol. Earth Syst. Sci. 15, 1167–1183.
Romilly, T., Gebremichael, M., 2011. Evaluation of satellite rainfall estimates over Ethiopian river basins. Hydrol. Earth Syst. Sci. 15, 1505–1514.
Saha, S., et al., 2010. The NCEP climate forecast system reanalysis. Bull. Am. Meteorol. Soc. 91, 1015.
Saha, S., et al., 2014. The NCEP climate forecast system version 2. J. Clim. 27, 2185–2208.
Saltelli, A., Tarantola, S., Chan, K.-S., 1999. A quantitative model-independent method for global sensitivity analysis of model output. Technometrics 41, 39–56.
Setegn, S.G., Srinivasan, R., Dargahi, B., 2008. Hydrological modelling in the Lake Tana Basin, Ethiopia using SWAT model. The Open Hydrology Journal 2 (1).

Sharma, S., Isik, S., Srivastava, P., Kalin, L., 2012. Deriving spatially distributed precipitation data using the artificial neural network and multilinear regression models. J. Hydrol. Eng. 18, 194–205.
SMHI, 2006. Integrated Hydrological Modelling System (IHMS). Manual Version 5.10. Swedish Meteorological and Hydrological Institute.
Steenhuis, T.S., et al., 2009. Predicting discharge and sediment for the Abay (Blue Nile) with a simple model. Hydrol. Process. 23, 3728–3737.
Steenhuis, T.S., et al., 2013. Simulating discharge and sediment concentrations in the increasingly degrading Blue Nile Basin. Proceedings Conference on Science and Technology Towards the Development of East Africa, pp. 291–299.
Steenhuis, T.S., et al., 2014. Soil erosion and discharge in the Blue Nile Basin: trends and challenges. Springer, Nile River Basin, pp. 133–147.
Tarekegn, D., Tadege, A., 2006. Assessing the Impact of Climate Change on the Water Resources of the Lake Tana Sub-Basin Using the WATBAL Model. CEEPA, University of Pretoria, Pretoria.
Taye, M.T., Willems, P., 2012. Temporal variability of hydroclimatic extremes in the Blue Nile basin. Water Resour. Res. 48.
Tesemma, Z.K., Mohamed, Y.A., Steenhuis, T.S., 2010. Trends in rainfall and runoff in the Blue Nile Basin: 1964–2003. Hydrol. Process. 24, 3747–3758.
Thornthwaite, C., Mather, J., 1955. The Water Balance. Centerton: Drexel Institute of Technology, 1955. 104p. Publications in Climatology 8.
Tian, Y., Peters-Lidard, C.D., Choudhury, B.J., Garcia, M., 2007. Multitemporal analysis of TRMM-based satellite precipitation products for land data assimilation applications. J. Hydrometeorol. 8, 1165–1183.
Tilahun, S., et al., 2013a. An efficient semi-distributed hillslope erosion model for the subhumid Ethiopian highlands. Hydrol. Earth Syst. Sci. 17, 1051–1063.
Tilahun, S., et al., 2013b. Asaturation Excess Erosion Model.
Wale, A., Rientjes, T., Gieske, A., Getachew, H., 2009. Ungauged catchment contributions to Lake Tana's water balance. Hydrol. Process. 23, 3682–3693.
Wang, W., et al., 2011. An assessment of the surface climate in the NCEP climate forecast system reanalysis. Clim. Dyn. 37, 1601–1620.
Whittaker, G., Confesor, R., Di Luzio, M., Arnold, J., 2010. Detection of overparameterization and overfitting in an automatic calibration of SWAT. Trans. ASABE 53, 1487–1499.
WMO, 1994. World Meteorological Organization Guide to Hydrological Practices: Data Acquisition and Processing, Analysis, Forecasting and Other Applications. GUIDE to Hydrological Practices, Geneva, p. 770.
Worqlul, A.W., et al., 2014. Comparison of rainfall estimations by TRMM 3B42, MPEG and CFSR with ground-observed data for the Lake Tana basin in Ethiopia. Hydrol. Earth Syst. Sci. 18, 4871–4881.
Xue, X., et al., 2013. Statistical and hydrological evaluation of TRMM-based multi-satellite precipitation analysis over the Wangchu Basin of Bhutan: are the latest satellite precipitation products 3B42V7 ready for use in ungauged basins? J. Hydrol. 499, 91–99.
Yilmaz, K.K., et al., 2005. Intercomparison of rain gauge, radar, and satellite-based precipitation estimates with emphasis on hydrologic forecasting. J. Hydrometeorol. 6, 497–517.
Zeleke, G., 2000. Landscape dynamics and soil erosion process modelling in the northwestern Ethiopian highlands.
Zulkafli, Z., et al., 2014. A comparative performance analysis of TRMM 3B42 (TMPA) versions 6 and 7 for hydrological applications over Andean–Amazon River basins. J. Hydrometeorol. 15, 581–592.